Fiber Optics Thermo Refractometer based on a Loose Cavity Design

Capstone Report

Zhalgaskhan Bakhytbek

Nazarbayev University
Department of Electrical and Computer Engineering
School of Engineering and Digital Sciences

This project report was created on TexStudio editing platform using LaTeX. All the figures were drawn using draw.io online software tool.

NAZARBAYEV UNIVERSITY

Electrical and Computer Engineering
Nazarbayev University
http://www.nu.edu.kz

Title:
Fiber Optics Thermo Refractometer based on a Loose Cavity Design

Theme:
Fiber Optic Sensors

Project Period:
Fall 2024 - Spring 2025

Project Group:
C4.208

Participant(s):
Zhalgaskhan Bakhytbek

Supervisor(s):
Carlo Molardi

Copies: 1

Page Numbers: 35

Date of Completion:
April 25, 2025

Abstract:

We describe the workings of a CFBG-based fiber-optic thermo-refractometer, including its design, construction, and experimental analysis. A resonant cavity was created by carefully cleaving a piece of single-mode fiber. This enhances sensitivity to changes in both temperature and refractive index (RI). The resonant-wavelength shift showed a linear response of 0.00926 nm/C with a coefficient of determination R^2 = 0.9962 during temperature calibration from 25C to 80C. We used an intensity-attenuation measure since the wavelength shifts in the RI calibration (5%-15% sucrose by weight, n=1.3477-1.3597) were inconsistent (R^2 = 0.11). By computing the mean of the filtered power within a 0.5 nm spectral band, we obtained a refractive-index sensitivity of –46.65 dB/RIU (R^2 = 0.9105). These findings show that in this loose-cavity CFBG setup, RI detection is robust when intensity modulation is used, and wavelength tracking is the best for temperature sensing.

Contents

Preface

This Capstone project investigates a loose-cavity chirped fiber Bragg grating thermo-refractometer for simultaneous temperature and refractive-index sensing. My motivation come from a deep interest in optical sensing and its applications in real-time environmental monitoring.

I am deeply grateful to Prof. Carlo Molardi for his guidance and to the laboratory team for granting access to the all of the equipment. Special thanks to my peers in group C4.208 for their guidance and feedback during laboratory works.

I declare that this report is my own work and that all sources have been acknowledged.

Nazarbayev University, April 25, 2025

Chapter 1

Introduction

Fiber-optic sensor (FOS) technology has developed significantly from its origin in the 1970s, beginning with first laboratory demonstrations and evolving to the first mass-produced sensors [1][2]. This evolution has been propelled by improvements in optoelectronic technology and an increasing comprehension of the distinctive features of optical fibers. The increasing use of FOS technology in areas such as structural monitoring, medical diagnostics, quality control systems, and industrial processes is a direct result of the technology's rapid advancements. [3][4][5].

The effectiveness of FOSs is based on their capacity to catch essential components of light, which is one of their main advantages. Fiber-optic sensors can measure strain, temperature, and pressure because light changes as it travels via an optical fiber [4][6]. Changes in wavelength, frequency, polarization, intensity, and phase are examples of light change. Each of these qualities can precisely identify physical property changes. By utilizing resonant cavities [7][8], fiber-optic sensors enhance their sensitivity and selectivity, allowing for precise detection of environmental changes at specific wavelengths. Increased sensitivity, resistance to electromagnetic interference, and multiplexing capability are unique features that make them important across several industries [3][9]. In addition, their small size and lightweight characteristics provide effortless incorporation into many architectures without significantly affecting the behavior of the monitored system.

Nowadays, many scientific and commercial applications require the ability to detect temperature-induced refractive index changes. In this case FOS thermo-refractometers are utilized. Understanding the relationship between temperature and refractive index is essential for using thermo-refractometers. Changes in temperatures affect material refractive indices, therefore precise measurement is needed in temperature management and monitoring systems. This is essential for proper temperature measurement. The observed patterns remain unsolved by standard models such as the Lorentz-Lorenz equation [10][11]. The link between liquid refractive index and temperature is complex. For an accurate wavelength-specific re-

fractive index estimate, temperature must be considered. Temperature gives more accurate refractive index measurements and is more reliable for chemical analysis and environmental monitoring.

Appropriate for many applications, fiber bragg gratings are among the most effective techniques for turning optical fibers into sensors [12][13][14]. A Fiber Bragg Grating (FBG) produced by introducing changes in the refractive index along the core of fiber. This modulation creates a Bragg-based selective filtering effect that reflects some wavelengths and transmits others. The reflected Bragg wavelength is sensitive to external conditions, especially temperature and strain [15]. The interaction between light and the grating structure provides this sensitivity since environmental changes affect the optical fiber. Refractive index and FBG grating period of optical fiber change with environmental factors. Two most common examples are mechanical strain and variations in temperature. Changing the reflected wavelength enables perfect measurement of given conditions [16]. This capability makes FBGs vital in applications like structural health monitoring and biomedical diagnostics, where accurate measurements are essential.

There are several types of Fiber Bragg Gratings, such as chirped [17], apodized [18], and tilted gratings [19]. The FBG gratings have different purposes and characteristics. This work will make advantage of chirped FBGs. CFBGs are perfect for thermo-refractometers for several reasons. First they provide spatially resolved grating length measurements and scattered sensing. In thermo-refractometry, this is crucial since temperature and refractive index vary over small distances [20]. Furthermore, because of their great sensitivity, CFBGs can find slight environmental changes. For some uses, this grating maximizes temperature and refractive index sensitivity. By lowering crosstalk between parameters, a non-uniform refractive index helps to simplify simultaneous measurements [20]. Moreover, CFBGs offer real-time data collecting in dynamic environments. Their small scale and adaptability for many systems make them perfect for thermo-refractometers. This industry likes CFBGs because of their consistent and accurate measurements.

This project work seeks to build a loose cavity design for fiber-optic sensors. This design's unique characteristics are used to improve performance parameters like measurement accuracy and response time without compromising modern sensor technologies' compactness and adaptability. The new method makes the proposed design an appropriate real-time multi-parameter sensing candidate for effective environment condition measurement.

1.1 Ethical and Professional Responsibilities

- **Ethical Responsibility:**
  Several ethical issues must be taken into account while developing and implementing a fiber-optic thermo-refractometer with a loose cavity design. One of the potential problems is making sure that the technology that is being used is both safe and appropriate. Environmental conditions in the biomedical or industrial domains, which need strict monitoring, are ideal for this system's application. To avoid damaging the environment or the users, it is necessary to follow safety measures under these conditions. This helps to make ensure the tools don't fail or have unexpected results.

  Moreover, another significant factor is the impact of the project on the surroundings, particularly with regard to resource use and disposal of electrical components. Minimizing the impact the project has on the surroundings depends on making sure the resources are obtained in an environmentally responsible manner and can be recycled sensibly. Should these moral concerns—safety and environmental responsibility—be addressed, the project can be launched in sync with both the growth of knowledge and society's values.

- **Informed Judgments:**
  Following these approaches will help us to ensure that the decisions made during the development of this project are well-informed:

  To get information on the current advancements and challenges in the field of fiber-optic sensing technology, first a thorough literature review and technical investigation will be conducted. By use of this fundamental information, the choice of materials and techniques will be guided, thereby ensuring that the project is based on accepted scientific ideas and progressive methods.

  Additionally, the project supervisor, who is very experienced in this area, will be included in the conversation regarding each and every phase of the project because of their expertise in this area. The feedback from the supervisor swill be helpful in evaluating the technological possibilities, which will ensure that they correspond not only with the requirements of the industry but also with the aims of the project. When progress is evaluated on a regular basis, it is possible to evaluate the degree to which decisions and technological goals are compatible with one another.

- **Global Context:**
  On a global scale, particularly in the many sectors directly affecting public health and environmental sustainability, the fiber-optic thermo-refractometer with a loose cavity design is quite relevant.

  In the field of environmental monitoring, for instance, this tool may measure the variations in refractive index and temperature in natural water bodies such as rivers and lakes[11]. By means of real-time data delivery, it helps assess the condition of the ecosystem and spot pollution, both of which are crucial for the preservation of aquatic life and the assurance of water free for human use. This use is especially pertinent in areas affected by industrial and agricultural runoff. This places are in need for water quality monitoring which is essential for the health of the inhabitants.

  In order to track temperature and refractive index simultaneously during chemical synthesis, the thermo-refractometer can be added into manufacturing configurations in industrial processes. This not only guarantees quality control and safety but also lessens the potential of dangerous reactions and the wasted material count. Through addressing worldwide issues of industrial safety and environmental damage, the fiber-optic thermo-refractometer can have positive effects over a broad spectrum of areas. Its uses might be catered to the particular needs and criteria of every location.

- **Economic Impact:**
  The development of a fiber-optic thermo-refractometer with a loose cavity architecture is poised to have major short-term and long-term economic effects across several sectors. Using this technology could help businesses like the oil and gas sector save money in the near future since they depend on accurate temperature and refractive index readings. For example, the performance of optical fiber sensors can be improved by utilizing this technology to detect asphaltene and wax formation in crude chemical compounds in high-pressure environments.[21]. Real-time data helps businesses to reduce downtime and stop expensive equipment breakdowns, so saving money right away.

  In many fields, including environmental sustainability, fiber-optic thermo-refractometers have transformative economic effects. For example, these sensors allow farmers to maximize irrigation systems and lower the amount of fertilizers thrown into nearby rivers by tracking the water quality in agricultural runoff. By encouraging ecologically friendly farming methods, the application of this technology offers the possibility to improve crop production. This will thereby protect important water supplies. This will result in a strengthening of the long-term agricultural output and sustainability. First implementation may face system integration and training challenges, but better efficiency, sustainability, and regulatory compliance may yield long-term

economic benefits in many areas.

- **Environmental Impact:**
  Application of this technology spans environmental monitoring, where it can be quite helpful in tracking changes in refractive index and temperature in sensitive environments. By placing the sensor in freshwater and marine habitats, for instance, researchers can spot early pollution signals and changes in ecosystem health. Maintaining biodiversity and guaranteeing the lifetime of natural environments depend on such frequent observation.

  Furthermore, as it was indicated in earlier sections of ethical obligations, the great sensitivity of sensors might have a major impact on sectors like environmental management and agriculture. Research on the interactions between materials and their surroundings can benefit from the fiber-optic thermo-refractometer, therefore promoting the growth of environmentally friendly substitutes in production techniques. Industries can create greener manufacturing methods by better knowing how materials react to different environments.

  All things considered, this project represents a dedication to environmental responsibility in addition to concentrating on accurate measuring possibilities. By means of eco-friendly methods and ecological monitoring applications, the thermo-refractometer supports a more sustainable future.

- **Societal Impact:**
  Some of the key advantages of the fiber-optic thermo-refractometer (FOTR) were covered in the other sections of Ethical and Professional Responsibilities. This new design will surely benefit society in one way or another. The fiber-optic thermo-refractometer can become necessary instrument for solving significant issues in environmental monitoring and healthcare since it can offer exact measurements in many uses.

  The fiber-optic thermo-refractometer's innovative design not only increases measuring accuracy but also ensures data reliability in many different fields. Whether in environmental assessments or therapeutic environments, this dependability helps to build more confidence in the data being applied to make important decisions.

  Furthermore encouraging multidisciplinary cooperation, the technology brings together experts in engineering, environmental science, and healthcare. Such cooperation can result in creative answers for challenging social problems, advancing technology, while responding to the needs of society.

  Using the fiber-optic thermo-refractometer has social consequences since it conforms with the ideas of improving environmental protection and human

welfare. Without a doubt, it is a great contribution to the technological terrain and a major benefit for society.

Chapter 2

Methodology

2.1 Sensor Design and Fabrication Procedure

For the best sensitivity for temperature and refractive index (RI) measurements, the fiber-optic thermo-refractometer with a loose cavity design was developed using a structured approach comprising sensor design, manufacturing, testing, and environmental validation.

To assess their applicability for usage in a thermo-refractometer, first several forms of Fiber Bragg Gratings (FBGs) were investigated: array of FBGs, apodized FBGs, and chirped FBGs (CFBGs). The most appropriate for this use, according to the results, were CFBGs as they had enhanced spectral bandwidth and great sensitivity to temperature and refractive index variations. For the loose cavity design, then, CFBGs were selected as they offered the optimum performance for the specified usage. The advantages of CFBGs were supported by findings from similar research, where the broad spectral response of chirped gratings allowed for simultaneous discrimination of temperature and refractive index changes with minimal cross-sensitivity between the two parameters [22].

To create the loose cavity, a section of the optical fiber was physically cut to form a precise gap which generates a resonant cavity. This cavity significantly enhances the interaction between the sensor and environmental changes by amplifying the reflected light signal, thereby increasing measurement sensitivity. The cutting was done using a fiber cleaver equipped with a diamond blade, which guaranteed clean and accurate cuts as shown in Figure 2.1.

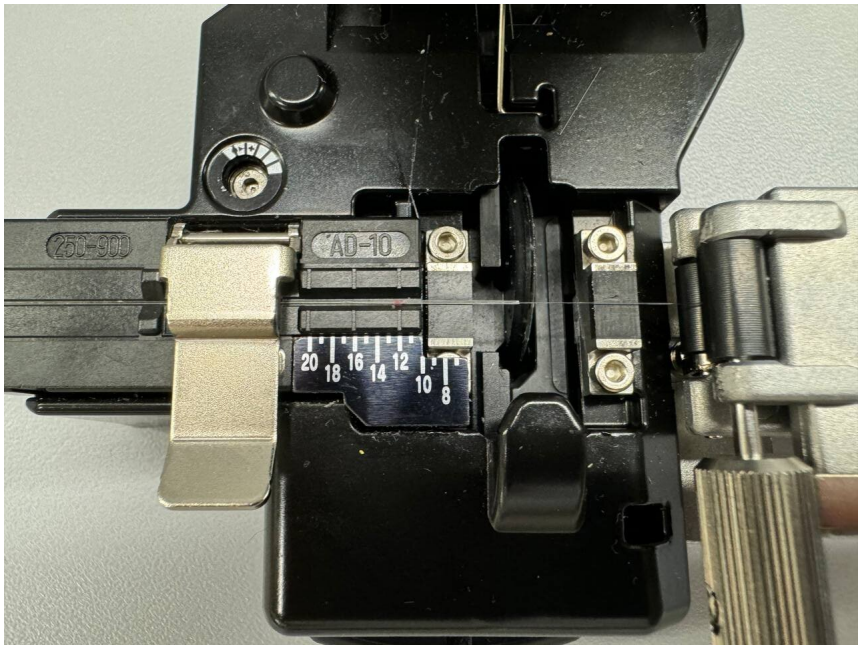

Figure 2.1: Diamond blade cleaver.

Prior to cleaving, the location was carefully measured and marked approximately 2.5 mm from the start of the grating section to get optimal spacing between the grating and the fiber-air interface. This ensured effective feedback from both the chirped grating reflector and the partial reflection at the cavity boundaries, forming an efficient resonant structure.

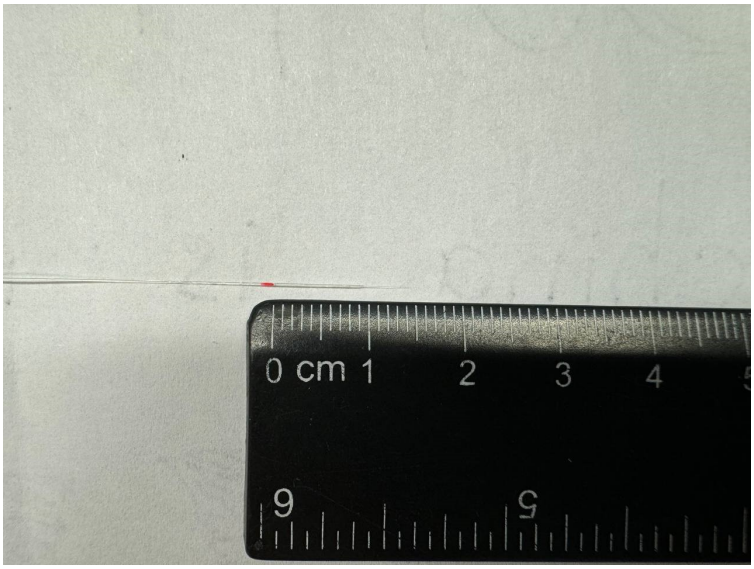

Figure 2.2: Precise marking of the optical fiber at a fixed distance (2.5 mm)

2.2 Micron Optics Hyperion si255 Interrogator

As seen in Figure 2.3, the primary data gathering platform for the CFBG-based thermo-refractometer's real-time interrogation was the Micron Optics Hyperion si255 optical interrogator, which was created by Luna Innovations' Micron Optics company. This instrument's multi-channel capabilities and high-speed wavelength scanning make it ideal for applications that demand dynamic spectral changes.

Figure 2.3: HYPERION si255.[23]

Introducing light into the sensor from a laser source operating in the 1520–1570 nm range allowed an optical spectrum analyzer (OSA) to capture the reflected spectra. A data collecting system was used to capture the changes in reflected wavelength under various environmental circumstances. According to official paper of product, the system is able to do static and dynamic full-spectrum analyses, allowing for accurate and dependable measurements taken over an extended period of time using over a thousand sensors spread out among sixteen parallel channels, each of which covers a wavelength range of 160 nm [23].

2.3 Temperature Calibration Experiment

A controlled thermal calibration experiment was carried out using a thermostatic water bath to check the temperature measurement sensitivity of the built sensor. The sensor was tested at a series of fixed temperature points, with each point being raised by 5°C, from 25°C to 80°C. At each temperature step, for optimal temperature balance, the sensor was placed in the water bath and to settle was left for a minimum of 3 minutes. As shown in Figure 2.4, the experimental setup included the water bath, the fiber-optic sensor mounted in a fixed position, and the connected Hyperion interrogation system.

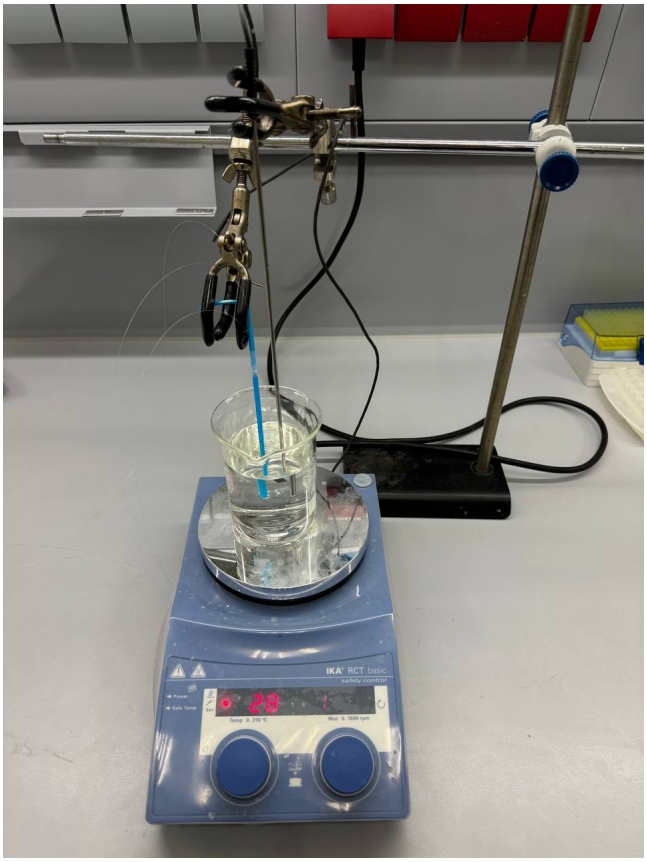

Figure 2.4: Experimental Setup for temperature testing.

The temperature value was carefully marked at each recorded spectrum. A magnetic stirrer was attached to the water bath to keep the temperature consistent and minimize variations in temperature.

2.4 Refractive Index Calibration Experiment

After the temperature test, the sensitivity to shifts in refractive index was evaluated using the same sensor. In this experiment, the sensor was placed in water with sucrose at various concentrations, increasing by 0.5 percent each time, from 10 percent to 15 percent by weight. The sensor remained in place and dipped in a tiny container of fluid. To reduce the effect of temperature fluctuation on RI measurements, the experiments took place in a thermally stable environment.

Figure 2.5: Experimental Setup for RI testing.

We can see the actual setup of the process in Figure 2.5. The fiber was connected to the Hyperion interrogator and placed in a container of calibrated solution. We exported the spectra and labeled them according to concentration once we repeated each experiment to ensure accuracy. Cleaning and wiping the sensor with distilled water after each test helped maintain it clear. It was done to prevent cross-contamination.

2.5 Methods and Procedure of Data Analysis

MATLAB was used in data analysis of this study to derive understanding from the spectrum data acquired during testing. MATLAB was imported the spectral data gleaned from the optical spectrum analyzer (OSA) for study. Extraction of the wavelength changes connected with temperature and refractive index came first. Understanding the reaction of the sensor to different environmental circumstances required knowledge of this kind.

Plotting the changes in wavelength relative to the determined temperature and refractive index values produced calibration curves. Linear regression analysis found sensitivity coefficients for refractive index and temperature. The sensitivity coefficients enabled a quantitative evaluation of the functioning of the sensor, therefore allowing later study and comparison.

The data was shown using MATLAB in the form of graphs and plots. It allowed for the detection of trends and relationships. To test the loose cavity design and investigate the sensor's behavior, we need to plot its spectrum response under different conditions. Repeated observations under the same environmental conditions confirms the sensor's reaction. It ensures consistency and reliability. In order to fix differences in the data, repeated measurements were carried out. The sensitivity of the sensor to changes in temperature and refractive index has been evaluated by sensitivity analysis. The derivation of sensitivity coefficients and evaluation of the linearity of sensor responses were both done with the use of MATLAB scripts. This allowed us to make an accurate assessment of the sensor's ability to differentiate between changes in refractive index and temperature.

2.6 Ethical Issues

The concept of integrity of data was fundamental during the entire research process. To ensure that we get consistent and accurate results, all experiments were conducted using calibrated instruments. In order to maintain transparency, we documented every step of data collection and analysis. The original data was never changed or modified in any way. Only in the case of signal processing and noise reduction. We recorded every change and stored the original datasets to allow independent verification if required. The aim was to guarantee that the study results were based on actual observations.

Public safety is impacted by the development of this project only in applications related to critical infrastructure. By helping in the better monitoring of structures including dams, bridges, and dams, the study aimed to enhance public safety. It was done to prevent structural disasters while maintaining an eye on accuracy and reliability.

Chapter 3

Results and Discussions

This study is defined by many experiments, including wavelength-to-power graphs for various types of Fiber Bragg Gratings (FBGs), temperature and refractive index measurements with three different chirped FBGs and their spectral response.

3.1 Comparison of FBG Types

First comparing FBGs, apodized FBGs, and chirped FBGs (CFBGs) involves creating wavelength-to-power graphs to evaluate their spectrum performance as shown in Figure 3.1. Every kind of FBG was tested under the same conditions.

The most fit for our fiber-optic thermo-refractometer was found to be CFBG. The findings revealed that CFBGs offered the optimum balance of spectral bandwidth and sensitivity. The variety of FBGs showed constant peaks throughout the spectrum, proving their dependability in pinpointing certain wavelengths. But compared to the CFBGs, the apodized FBGs—which included suppressed sidelobes—offers a less strong reflecting signal. Conversely, the most complete spectrum response with wider bandwidth provided by the CFBGs allowed for reliable detection of both temperature and refractive index changes, therefore enabling multiparameter sensing.

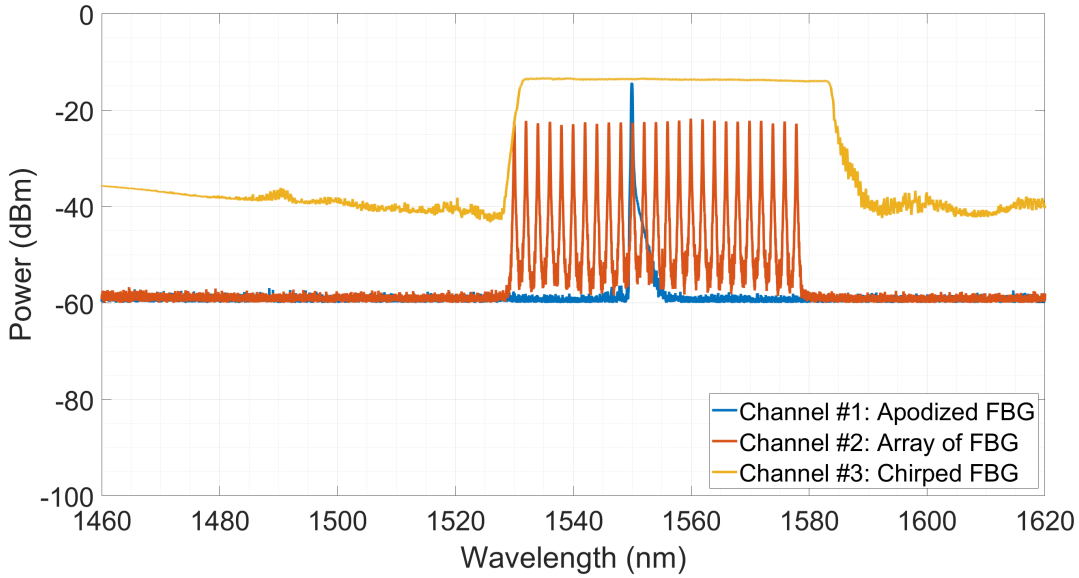

Figure 3.1: Comparison of FBG Types.

3.2 Temperature experiment

For temperature measurement experiments, three different CFBGs, identified by their serial numbers (CFBG Serial Number 101122404010, CFBG Serial Number 101121708004, and CFBG Serial Number 101082005011), were tested before and after being cut to form the loose cavity. The figures of the three fibers before and after cutting can be seen in Figures 3.2 to 3.4. This process involved careful analysis of the reflected wavelength shifts before and after the cutting procedure. Graphs depicting the spectral responses before cutting indicated strong, distinct reflection peaks, whereas after cutting, the response became a single peak due to the increased interaction length within the cavity. These shifts confirmed that the loose cavity design effectively enhanced the sensor's sensitivity by allowing the light to interact more with the surrounding environment, thereby improving the sensor's ability to detect minute changes in temperature and refractive index.

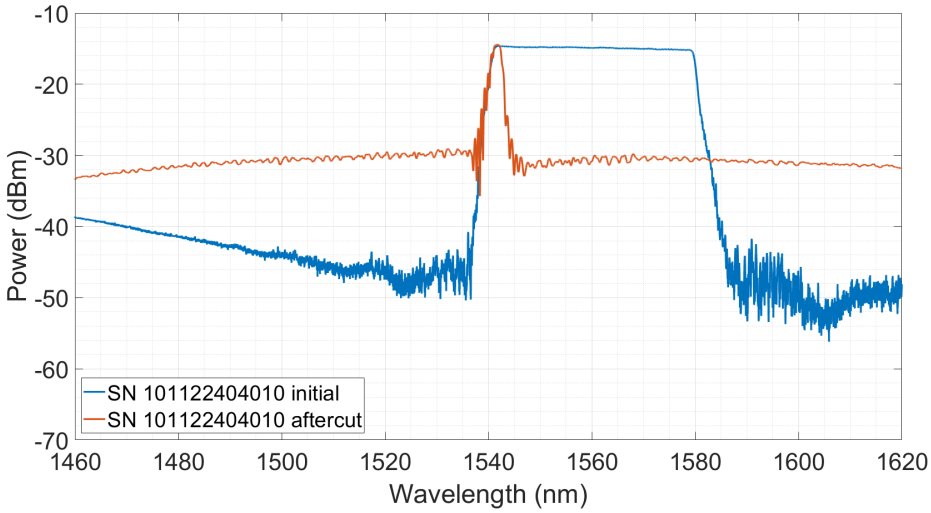

Figure 3.2: CFBG Serial Number 101122404010.

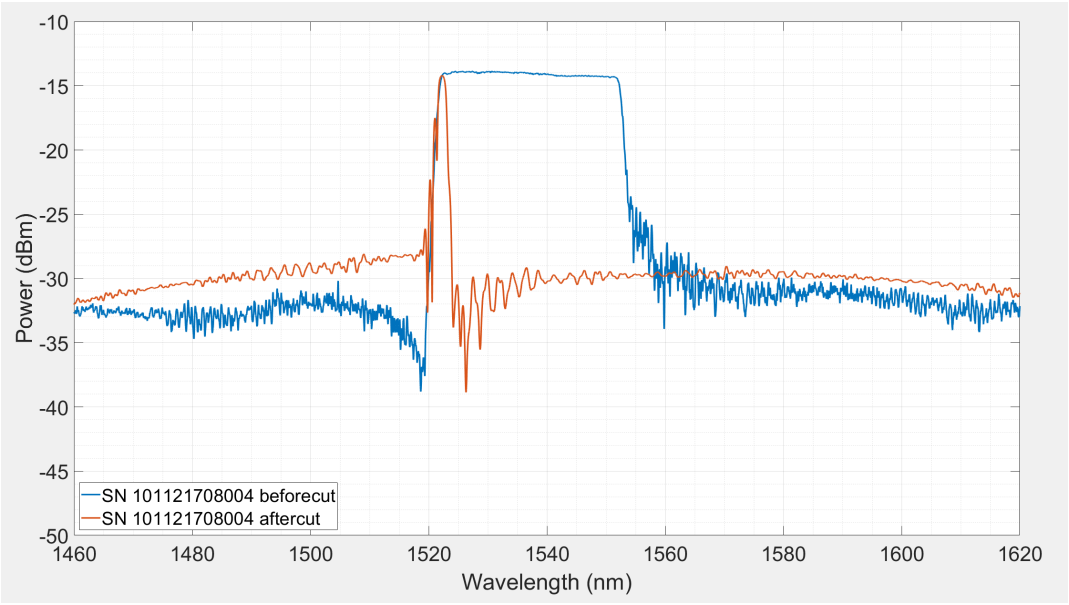

Figure 3.3: CFBG Serial Number 101121708004.

Figure 3.4: CFBG Serial Number 101082005011.

The three CFBGs were merged into many channels for the performance testing in a real-world environment during the primary experimental phase. Channel 1 connects specifically to Serial Number 101121708, Channel 2 to Serial Number 101082005, and Channel 3 to Serial Number 10108200500. The experiment consisted on progressively raising the temperature from 25°C to 80°C under observation of every sensor channel. Every CFBG underwent real-time monitoring and spectral change logging by means of the Micron Optics Hyperion si255 system.

Channel 1 (CFBG Serial Number 101121708004): Channel 1 connects under CFBG Serial Number 101121708004. Unfortunately, useless data came from a mistake made during data collection for this channel. The mistake came from a hand cut of the fiber done without a diamond cleaver. The inaccurate cut produced poor optical coupling and signal quality, therefore rendering the data unreliable. As can be seen in Figure 3.5, the relationship between temperature and wavelength shift in Channel 1 is not linear, further demonstrating the impact of the incorrect cut. This emphasizes the need of maintaining sensor integrity and guaranteeing exact cuts by use of a diamond cleaver.

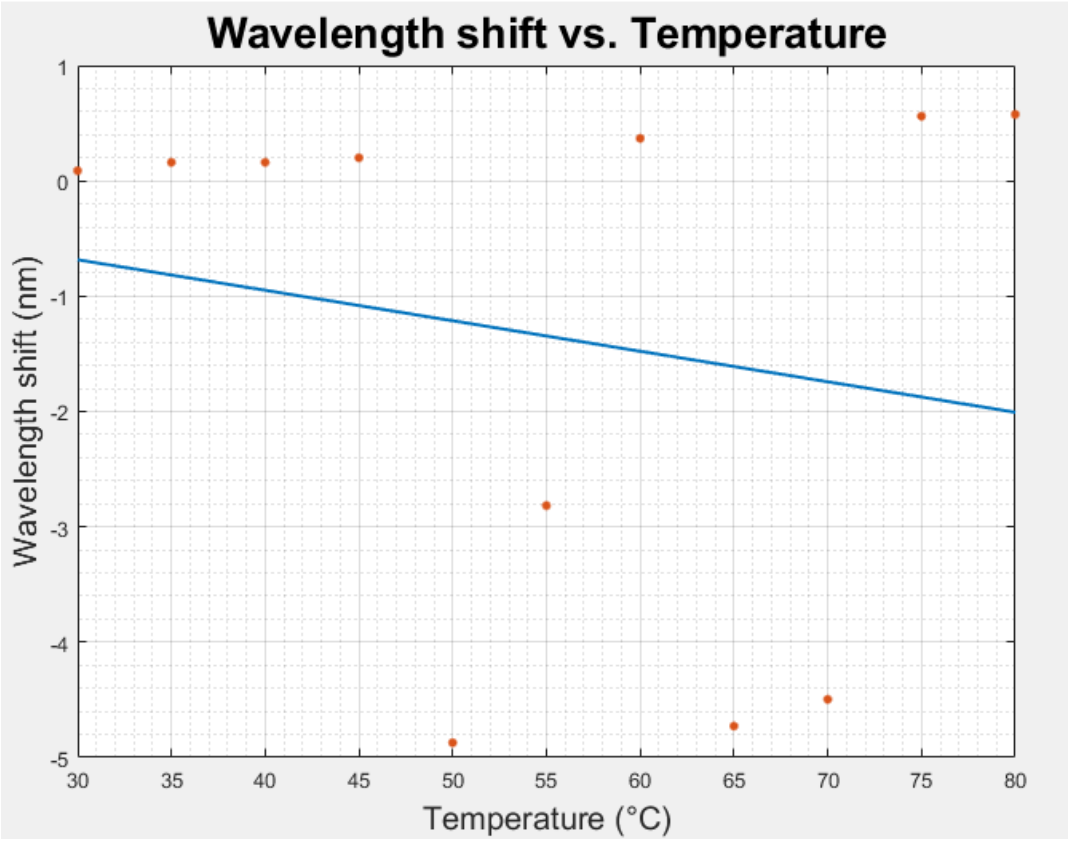

Figure 3.5: Channel 1 – incorrect response.

Channel 2 (CFBG Serial Number 101082005011): Channel 2 connects under CFBG Serial Number 101082005011. Successful measurements for this channel revealed a strong linear link between temperature and wavelength shift. The reflected wavelength moved linearly from 25°C to 80°C, suggesting a significant relationship between the external temperature and the Bragg wavelength. As Figure 3.6 shows, the connection between temperature and wavelength is nearly linear. Moreover, Channel 2's spectral response graph which shown in Figure 3.7 revealed clear reflection peaks that moved proportionately with rising temperature, therefore verifying the accuracy of the sensor in tracking temperature variations.

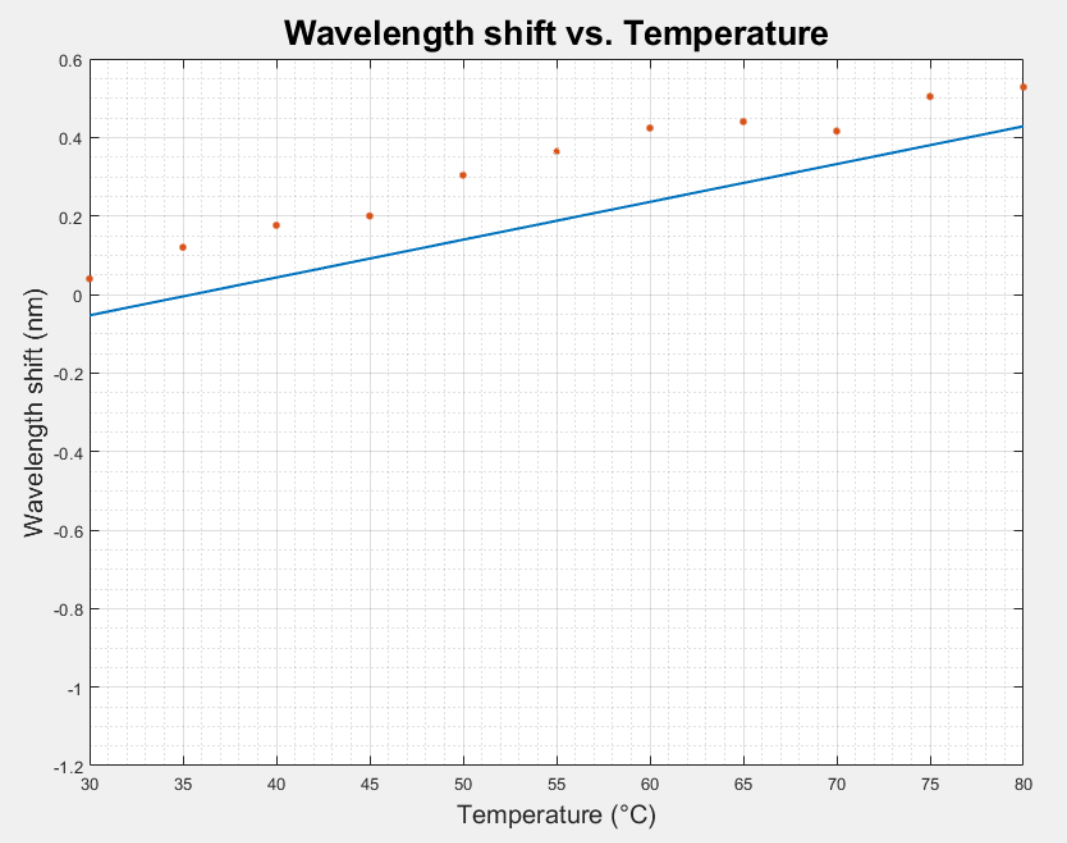

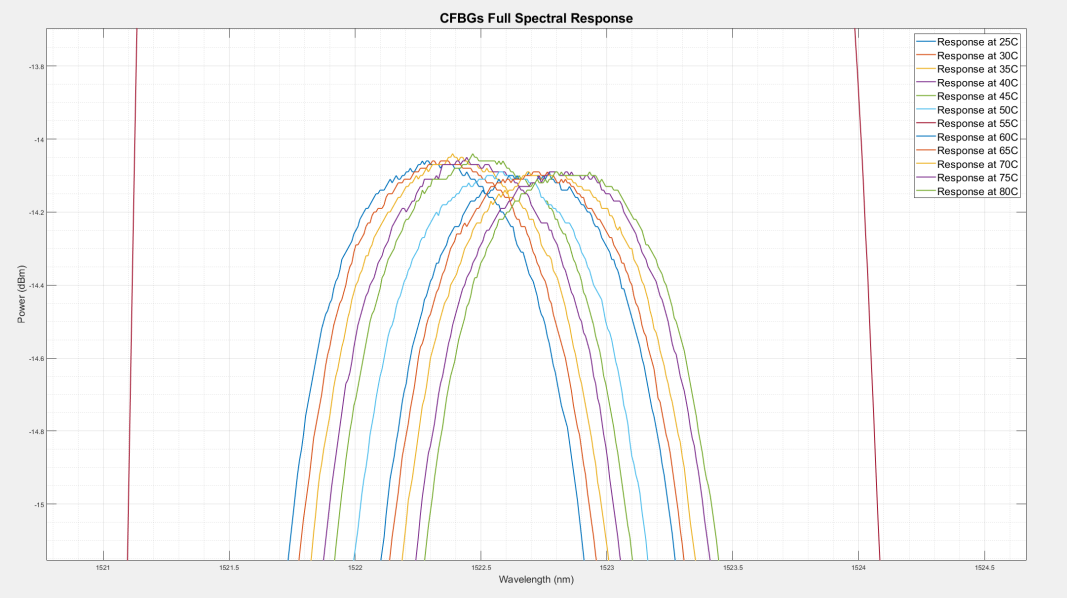

Figure 3.7: Channel 2 – Spectral Response.

Channel 3 (CFBG Serial Number 101122404010): Channel 3's measures were the most steady and accurate. With the wavelength rising as the temperature ascended, the findings revealed a linear link between temperature and wavelength change. With only small differences likely caused by experimental factors, its temperature response showed a nearly perfect linear relationship between Bragg wavelength and temperature rise. Figure 3.8 shows that, for Channel 3, the connection between temperature and wavelength is ideal linear. The Micron Optics Hyperion si255 system's excellent resolution let us precisely follow the spectrum changes that are shown in Figure 3.9.

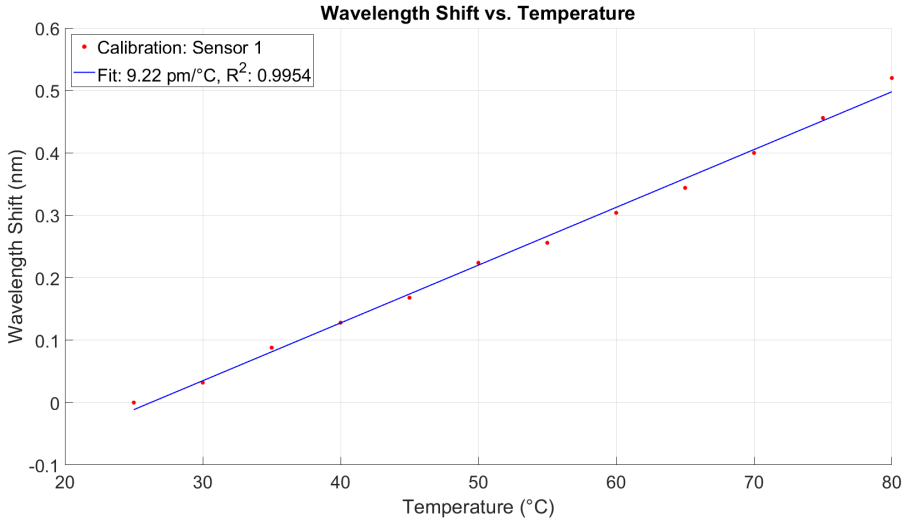

Figure 3.8: Channel 3 – Wavelength shift.

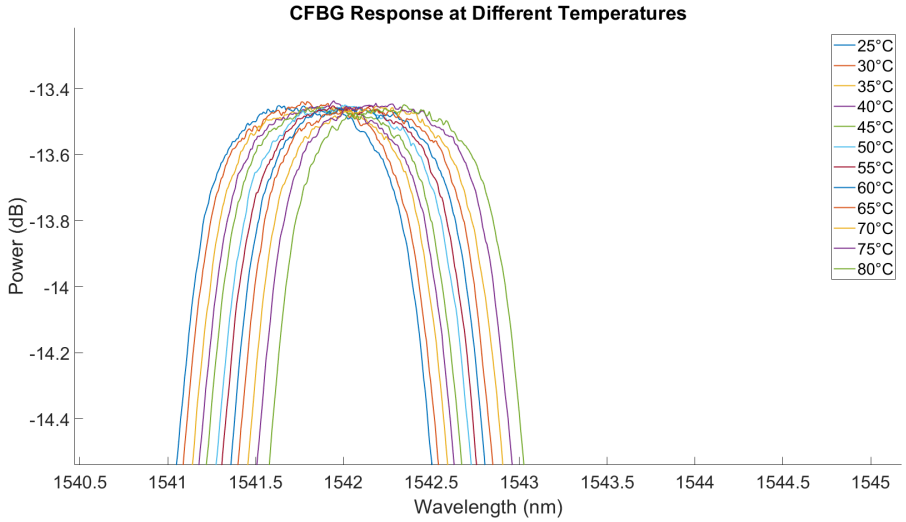

Figure 3.9: Channel 3 – Spectral Response.

3.3 Refraction Index (RI) experiment

The next step, after the temperature calibration tests, was to determine how the sensor would react to variations in the refractive index (RI). Further RI testing was carried out on CFBG SN-101122404010 due to its linear temperature sensitivity and very consistent results. After verification of its exceptional signal accuracy and consistency in the temperature tests outlined in Section 3.2, this sensor was chosen for our next investigation.

Apart from temperature readings, the sensors underwent evaluation concerning their reaction to variations in refractive index. These tests were carried out in air and by submerging the sensors in fluids with varying refractive indices between 10 and 15 percent sucrose concentration. The sensitivity to refractive index was measured and can be seen in the figure below.

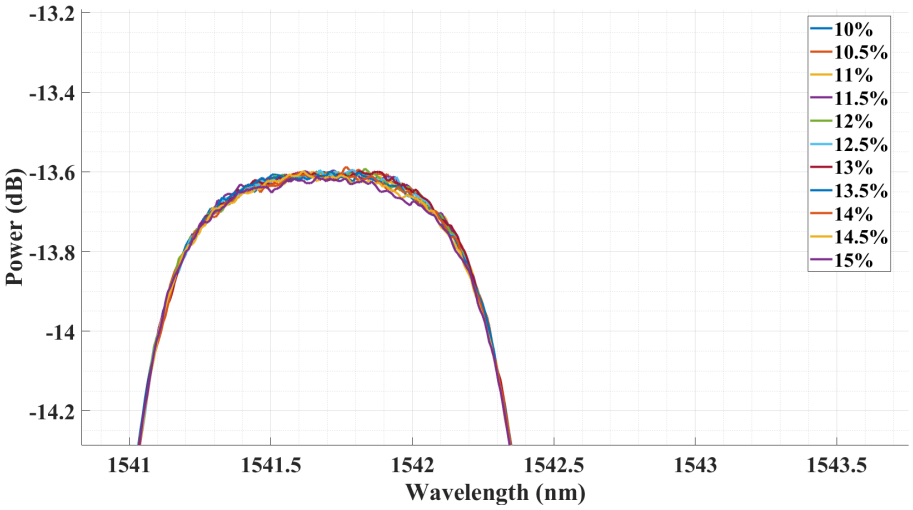

Figure 3.10: Spectral Response to RI change.

Although there were small changes in the reflected power and peak location, the spectral response was quite stable throughout a wide range of refractive index (RI) values, indicating a slight but noticeable sensitivity to RI changes.

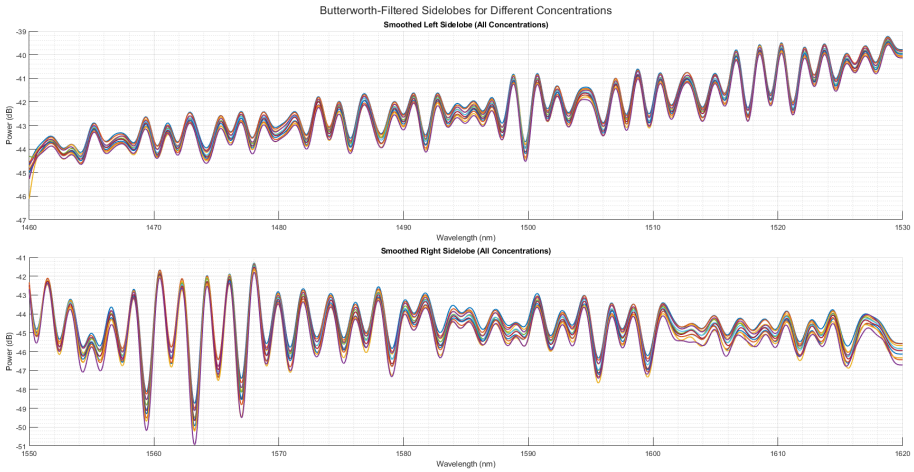

Figure 3.11: Butterworth-Filtered Sidelobes for Different Concentrations.

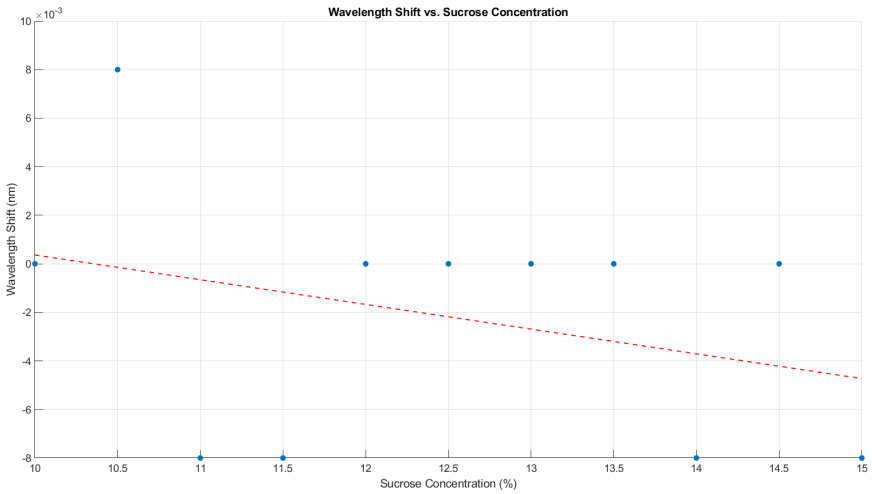

Figure 3.12: Wavelength Shift.

Additional information on the sensor's response to changes in refractive index can be seen in Figures 3.11 and 3.12. Spectra of the Butterworth-filtered sidelobes with different concentrations of sucrose are shown in Figure 3.11. In addition to a stable overall spectral shape, the smoothed curves show that the intensity of the the sidelobes varies a bit with increasing concentration. These signs give confidence to the trend of decreasing reflected power as RI values rise.

In contrast, Figure 3.12 illustrates the wavelength shift of the main peak with respect to sucrose concentration. The shift values fluctuate across the concentration range, which indicates that wavelength shift does not serve as a reliable indicator of refractive index in this set.

3.4 Discussion

There was a strong and nearly direct relationship between environmental temperature and Bragg wavelength shift as shown in the temperature calibration experiments. When compared to the other CFBGs that were tested, the CFBG with SN-101122404010 had the best spectrum stability and consistency.

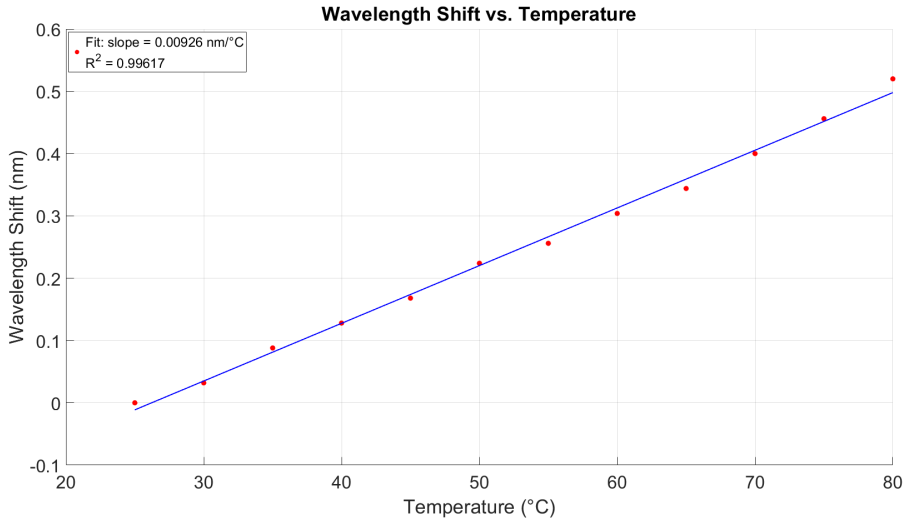

Figure 3.13: Coefficient of determination and Sensitivity.

The best-performing sensor, resulted a sensitivity of 0.00926 nm/°C and an R^2 value of 0.99617, as shown in Figure 3.13. This points to a wavelength shift of about 9.26 picometers per degree Celsius, which is consistent across all points of measurement. The sensor's is suitable for precise thermal monitoring applications.

The same sensor was then tested in settings with different refractive indices by submerging it in sucrose solutions with concentrations ranging from 10 percent to 15 percent. The refractive indices that they correspond to range from around 1.3477 to 1.3597.

The refractive index response of the sensor was evaluated by plotting the wavelength shift of the reflection peak against sucrose concentration. Results from the linear fit showed a low coefficient of determination (R^2 = 0.1065) and a sensitivity of -0.0010. This indicates the relationship between sucrose concentration and Bragg wavelength shift is weak and inconsistent. It can be due to weak coupling between the external refractive index and the Bragg reflection peak position.

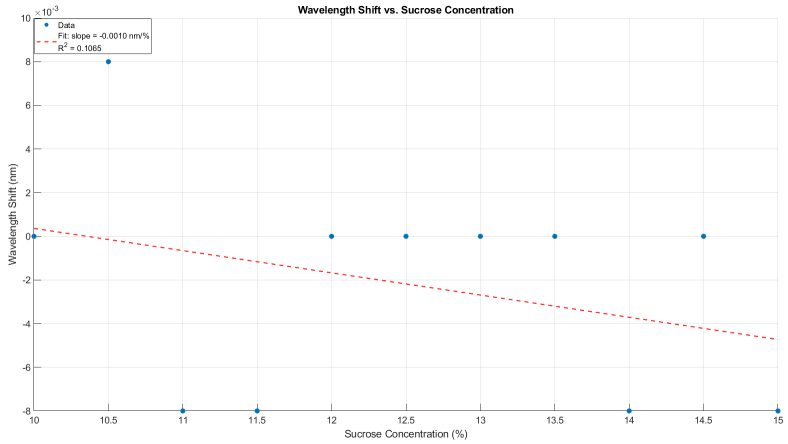

Figure 3.14: Coefficient of determination and Sensitivity.

We switched our focus to examining the attenuation in reflected power across various sucrose concentrations because the wavelength data did not show any relevant association. For each concentration step, the average power was retrieved within a limited wavelength window (1512.6-1513.1 nm). We were able to do a linear fit and calculate the sensitivity (dP/RIU) due to this method, which showed a consistent trend. The enhanced R^2 value and the consequent slope showed that intensity-based detection was better than wavelength shift for tracking changes in the refractive index in this setup.

This method resulted a sensitivity of dP/RIU = –46.6451, with a strong correlation coefficient of R^2 = 0.9105. These results confirm that intensity-based sensing is more robust and reliable for refractive index detection in this CFBG-based loose cavity sensor compared to wavelength shift analysis.

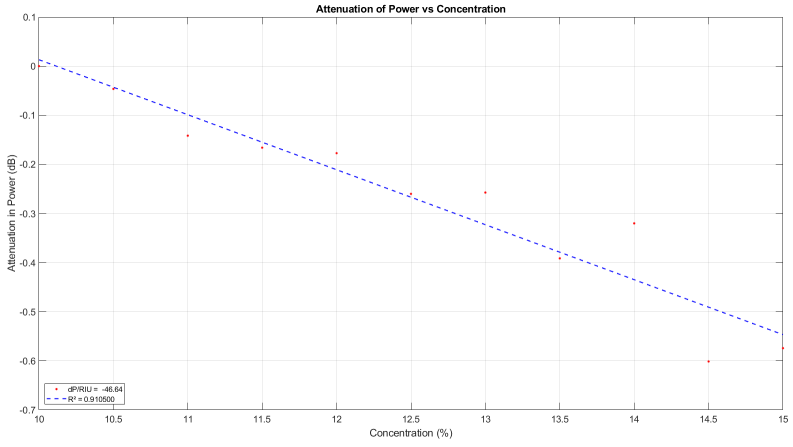

Figure 3.15: Attenuation in Power vs Concentration of Sucrose.

Chapter 4

Conclusion

This study demonstrated the development and experimental verification of a fiber-optic thermo-refractometer that uses a chirped fiber Bragg grating (CFBG) in a loose cavity configuration. The sensor's strong steady temperature sensitivity proved that the cavity-enhanced grating construction performed as intended. A better indication of RI shifts was obtained by switching to power attenuation analysis from monitoring wavelength shifts, the original method of refractive index sensing, which produced inconsistent findings.

The results show that the sensor can detect two parameters at once: temperature and refractive index. The first can be measured precisely by spectrum shifts, while the latter can be better seen by intensity modulation. To further enhance detection sensitivity and linearity, further enhancements might involve improving the cavity length and cleaving accuracy, improving the signal processing approaches, and investigating larger refractive index ranges.

Bibliography

[1] Eric Udd. "An overview of fiber-optic sensors". In: *Review of Scientific Instruments* 66.8 (Aug. 1995), pp. 4015–4030. DOI: 10.1063/1.1145411. URL: https://doi.org/10.1063/1.1145411.

[2] K.T.V. Grattan and T. Sun. "Fiber optic sensor technology: an overview". In: *Sensors and Actuators A: Physical* 82.1 (2000), pp. 40–61. ISSN: 0924-4247. DOI: https://doi.org/10.1016/S0924-4247(99)00368-4. URL: https://www.sciencedirect.com/science/article/pii/S0924424799003684.

[3] Wolfgang R. Habel and Katerina Krebber. "Fiber-optic sensor applications in civil and geotechnical engineering". In: *Photonic Sensors* 1.3 (Mar. 2011), pp. 268–280. DOI: 10.1007/s13320-011-0011-x.

[4] Bahareh Gholamzadeh and Hooman Nabovati. "Fiber optic sensors". In: *International Journal of Electronics and Communication Engineering* 2.6 (2008), pp. 1107–1117.

[5] Daniele Tosi et al. "Fiber optic sensors for sub-centimeter spatially resolved measurements: Review and biomedical applications". In: *Optical Fiber Technology* 43 (Mar. 2018), pp. 6–19. DOI: 10.1016/j.yofte.2018.03.007. URL: https://doi.org/10.1016/j.yofte.2018.03.007.

[6] Tiange Wu et al. "Recent progress of fiber-optic sensors for the structural health monitoring of civil infrastructure". In: *Sensors* 20.16 (2020), p. 4517. DOI: 10.3390/s20164517.

[7] Rüdiger Paschotta. "optical resonators". In: (Sept. 2024). URL: https://www.rp-photonics.com/optical_resonators.html.

[8] Rüdiger Paschotta. "cavities". In: (Sept. 2024). URL: https://www.rp-photonics.com/cavities.html.

[9] Muhammad Arif Riza et al. "FBG sensors for environmental and biochemical applications—A review". In: *IEEE sensors journal* 20.14 (2020), pp. 7614–7627. DOI: 10.1109/JSEN.2020.2982446.

[10] D. Beysens and P. Calmettes. "Temperature dependence of the refractive indices of liquids: Deviation from the Lorentz–Lorenz formula". In: *The Journal of Chemical Physics* 66.2 (Jan. 1977), pp. 766–771. DOI: 10.1063/1.433954. URL: https://doi.org/10.1063/1.433954.

[11] J. J. Imas et al. "Optical fiber thermo-refractometer". In: *Optics Express* 30.7 (Feb. 2022), p. 11036. DOI: 10.1364/oe.450316. URL: https://doi.org/10.1364/oe.450316.

[12] "Application of FBG sensors for geotechnical health monitoring, a review of sensor design, implementation methods and packaging techniques". In: *Sensors and Actuators A: Physical* 244 (2016), pp. 184–197. ISSN: 0924-4247. DOI: https://doi.org/10.1016/j.sna.2016.04.033.

[13] Gayan C. Kahandawa et al. "Use of FBG sensors for SHM in aerospace structures". In: *Photonic Sensors* 2.3 (July 2012), pp. 203–214. DOI: 10.1007/s13320-012-0065-4. URL: https://doi.org/10.1007/s13320-012-0065-4.

[14] "Development of a long-term monitoring system based on FBG sensors applied to concrete bridges". In: *Engineering Structures* 32.8 (2010), pp. 1993–2002. ISSN: 0141-0296. DOI: https://doi.org/10.1016/j.engstruct.2010.02.033.

[15] Rüdiger Paschotta. "fiber Bragg gratings". In: (Sept. 2024). URL: https://www.rp-photonics.com/fiber_bragg_gratings.html.

[16] Jinjie Chen, Bo Liu, and Hao Zhang. "Review of fiber Bragg grating sensor technology". In: *Frontiers of Optoelectronics in China* 4.2 (June 2011), pp. 204–212. DOI: 10.1007/s12200-011-0130-4.

[17] Daniele Tosi. "Review of Chirped Fiber Bragg Grating (CFBG) Fiber-Optic Sensors and their applications". In: *Sensors* 18.7 (July 2018), p. 2147. DOI: 10.3390/s18072147.

[18] I. Ashry et al. "Investigating the performance of apodized Fiber Bragg gratings for sensing applications". In: (2014), pp. 1–5. DOI: 10.1109/ASEEZone1.2014.6820640.

[19] Jacques Albert, Li-Yang Shao, and Christophe Caucheteur. "Tilted fiber Bragg grating sensors". In: *Laser and Photonics Review* 7.1 (Feb. 2012), pp. 83–108. DOI: 10.1002/lpor.201100039.

[20] M. Shaimerdenova et al. "An etched chirped fiber Bragg grating for measurement of refractive index and temperature pattern". In: 10820 (2018). Ed. by Qingming Luo et al., 108203B. DOI: 10.1117/12.2502471.

[21] Jimmy Castillo et al. “Optical fiber extrinsic refractometer to measure RI of samples in a high pressure and temperature systems: Application to wax and asphaltene precipitation measurements”. In: *Fuel* 85.14 (2006), pp. 2220–2228. ISSN: 0016-2361. DOI: https://doi.org/10.1016/j.fuel.2006.03.020. URL: https://www.sciencedirect.com/science/article/pii/S0016236106000895.

[22] Takhmina Ayupova, Madina Shaimerdenova, and Daniele Tosi. “Shallow-tapered chirped fiber Bragg grating sensors for dual refractive index and temperature sensing”. In: *Sensors* 21.11 (2021), p. 3635.

[23] “HYPERION si255”. In: (). URL: https://lunainc.com/product/hyperion-si255.

Appendix A

Appendix A Matlab Code

```
close all
clear
clc

delimiterIn = '\t';
headerlinesIn = 70;
x_wavelength = linspace(1460, 1620, 20000);

% Importing data from txt files
filename_1 = 'Spectral Response Before Cut SN -101122404010 (2).txt';
filename_2 = 'Spectral Response After Cleaving SN -101122404010 (2).txt';

CFBG_SN_101122404010_initial = importdata(filename_1, delimiterIn, headerlinesIn);
CFBG_SN_101122404010_aftercut = importdata(filename_2, delimiterIn, headerlinesIn);

% Collecting response data
FullRes_101122404010_initial = CFBG_SN_101122404010_initial.data(1, :);
FullRes_101122404010_aftercut = CFBG_SN_101122404010_aftercut.data(1, :);

% Plotting spectral responses
figure('Name', 'CFBG SN-101122404010 Spectral Response');
plot(x_wavelength, FullRes_101122404010_initial, 'LineWidth', 2.5);
hold on
```

```
24          plot(x_wavelength, FullRes_101122404010_aftercut, '
                LineWidth', 2.5);
25          hold off
26
27          xlim([1460 1620]);
28          ylim([-70 -10]);
29
30          legend({'SN␣101122404010␣Initial','SN␣101122404010␣
                After␣Cut'}, 'Location', 'southwest');
31          xlabel('Wavelength␣(nm)');
32          ylabel('Power␣(dBm)');
33          set(gca, 'fontsize', 32);
34          grid on;
35          grid minor;
```

Listing A.1: Plotting of spectral graphs.

```
1           close all;
2           clear
3           clc
4
5           filenames = { '25_1.txt', '30_1.txt', '35_1.txt', '40_1
                .txt', '45_1.txt', '50_1.txt', ...
6                   '55_1.txt', '60_1.txt', '65_1.txt', '70_1.txt',
                        '75_1.txt', '80_1.txt' };
7
8           num_files = length(filenames);
9           colors = lines(num_files);
10          temperature_labels = 25:5:80;
11          wavelengths = cell(num_files, 1);
12          power_values = cell(num_files, 1);
13
14          %% Spectral responses
15          figure; hold on;
16          for i = 1:num_files
17          data = readmatrix(filenames{i});
18          wavelengths{i} = data(:, 1);
19          power_values{i}    = data(:, 2);
20          plot(wavelengths{i}, power_values{i}, 'Color', colors(i
                , :), 'LineWidth', 1.5);
21          end
22          hold off;
23          xlabel('Wavelength␣(nm)', 'FontSize', 24);
24          ylabel('Power␣(dB)', 'FontSize', 24);
25          title('CFBG␣Response␣at␣Different␣Temperatures', '
                FontSize', 24);
26          legend(arrayfun(@(x) sprintf('', x), temperature_labels
```

```
    , 'UniformOutput', false));
set(gca, 'FontSize', 24);

%% Threshold intersections
max_powers      = cellfun(@max, power_values);
avg_max_power   = mean(max_powers);
threshold_power = avg_max_power - 1;

intersection_wavelengths = NaN(num_files, 1);
for i = 1:num_files
idx = find(power_values{i} >= threshold_power, 1, '
    first');
if ~isempty(idx)
intersection_wavelengths(i) = wavelengths{i}(idx);
end
end

%% Wavelength shifts
reference_wavelength = intersection_wavelengths(1);  25
    C as reference
wavelength_shifts    = intersection_wavelengths -
    reference_wavelength;
disp('Temperature␣(C)␣|␣Intersection␣Wavelength␣(nm)␣|␣
    Wavelength␣Shift␣(nm)');
disp([temperature_labels', intersection_wavelengths,
    wavelength_shifts]);


p = polyfit(temperature_labels, wavelength_shifts, 1);
sensitivity = p(1);
fit_shifts = polyval(p, temperature_labels);
R = corrcoef(temperature_labels, wavelength_shifts);
R_squared_alt = R(1,2)^2;
%% Plot Wavelength Shift vs. Temperature with legend
figure;
scatter(temperature_labels, wavelength_shifts, 50, 'r',
     'filled');
hold on;
fit_temps  = linspace(min(temperature_labels), max(
    temperature_labels), 100);
fit_curve  = polyval(p, fit_temps);
plot(fit_temps, fit_curve, 'b-', 'LineWidth', 1.5);
hold off;

xlabel('Temperature␣(C)', 'FontSize', 24);
ylabel('Wavelength␣Shift␣(nm)', 'FontSize', 24);
title('Wavelength␣Shift␣vs.␣Temperature', 'FontSize',
```

```
    24);
set(gca, 'FontSize', 24);
grid on;
legend(...
sprintf('Fit: slope = .5f nm/C\nR^2 = .5f', sensitivity
    , R_squared_alt), ...
'Location', 'best', ...
'FontSize', 18 ...
);
```

Listing A.2: Temperature Data Processing.

```
close all
clear
clc

filenames = { 'RI1_1.txt', 'RI2_1.txt', 'RI3_1.txt', '
    RI4_1.txt', 'RI5_1.txt', 'RI6_1.txt', ...
        'RI7_1.txt', 'RI8_1.txt', 'RI9_1.txt', 'RI10_1.
            txt', 'RI11_1.txt'};

num_files = length(filenames);
colors = lines(num_files);
concentration_labels = 10:0.5:15;
wavelengths = cell(num_files, 1);
power_values = cell(num_files, 1);

figure; hold on;
for i = 1:num_files
data = readmatrix(filenames{i});

wavelengths{i} = data(:, 1);
power_values{i} = data(:, 2);


plot(wavelengths{i}, power_values{i}, 'Color', colors(i
    , :), 'LineWidth', 3);
end
ylim([-60 0]);
hold off;

xlabel('Wavelength (nm)');
ylabel('Power (dB)');
legend(arrayfun(@(x) sprintf('%g%%', x),
    concentration_labels, 'UniformOutput', false), ...
'Location', 'best');
set(gca,'FontName', 'Times New Roman', 'FontWeight','
```

```
        bold', 'FontSize', 30);

    grid on
    grid minor
```

Listing A.3: RI data processing.

```
close all;
clear;
clc;

filenames = { 'RI1_1.txt', 'RI2_1.txt', 'RI3_1.txt', 'RI4_1.txt', 'RI5_1.txt', 'RI6_1.txt', ...
        'RI7_1.txt', 'RI8_1.txt', 'RI9_1.txt', 'RI10_1.txt', 'RI11_1.txt'};
num_files            = length(filenames);
concentration_labels = 10:0.5:15;  % in %

right_sidelobe_range = [1570, 1620];
order        = 5;
cutoff_freq  = 0.01;
[b, a]       = butter(order, cutoff_freq, 'low');
peak_wavelengths = NaN(num_files,1);

for i = 1:num_files
data          = readmatrix(filenames{i});
wavelengths   = data(:,1);
power_values  = data(:,2);

idx     = wavelengths >= right_sidelobe_range(1) & wavelengths <= right_sidelobe_range(2);
wl_sub  = wavelengths(idx);
pw_sub  = power_values(idx);
smooth_pw = filtfilt(b, a, pw_sub);
[peaks, locs] = findpeaks(smooth_pw, wl_sub);
if ~isempty(peaks)
[~, maxIdx]           = max(peaks);
peak_wavelengths(i) = locs(maxIdx);
end
end

disp('Concentration␣(%)␣␣␣␣Peak␣Wavelength␣(nm)');
disp([concentration_labels', peak_wavelengths]);

ref_wl            = peak_wavelengths(1);
wavelength_shifts = peak_wavelengths - ref_wl;
p                 = polyfit(concentration_labels,
```

```
            wavelength_shifts, 1);
38          sensitivity     = p(1);
39          R               = corrcoef(concentration_labels,
                wavelength_shifts);
40          R_squared_alt   = R(1,2)^2;
41
42          fprintf('Sensitivity: sensitivity);
43  ␣␣␣␣␣␣␣␣fprintf('R   (corrcoef): R_squared_alt);
44          figure;
45          scatter(concentration_labels, wavelength_shifts, 60, '
                filled');
46          hold on;
47          x_fit = linspace(min(concentration_labels), max(
                concentration_labels), 100);
48          y_fit = polyval(p, x_fit);
49          plot(x_fit, y_fit, 'r--', 'LineWidth', 1.5);
50          hold off;
51
52          xlabel('Sucrose Concentration ()', 'FontSize', 16);
53          ylabel('Wavelength Shift (nm)',        'FontSize', 16);
54          title('Wavelength Shift vs. Sucrose Concentration', '
                FontSize', 18);
55          grid on;
56          set(gca,'FontSize',14);
57
58          legend( ...
59          'Data', ...
60          sprintf('Fit: slope = %.4f nm/%%\nR^2 = %.4f',
                sensitivity, R_squared_alt), ...
61          'Location','best', 'FontSize',12 ...
62          );
```

Listing A.4: Wavelength Shift vs. Sucrose Concentration.

```
1           close all; clear; clc;
2
3           files = { ...
4                   'RI1_1.txt','RI2_1.txt','RI3_1.txt','RI4_1.txt'
                        ,'RI5_1.txt', ...
5                   'RI6_1.txt','RI7_1.txt','RI8_1.txt','RI9_1.txt'
                        ,'RI10_1.txt','RI11_1.txt' ...
6           };
7           nFiles      = numel(files);
8           leftRange   = [1460, 1530];
9           rightRange  = [1550, 1620];
10          [b,a]       = butter(5, 0.01, 'low');
11
```

```
12          figure;
13          tiledlayout(2,1,'TileSpacing','compact');
14
15          ax1 = nexttile;
16          hold(ax1,'on');
17          for i = 1:nFiles
18          data    = readmatrix(files{i});
19          wl      = data(:,1);
20          pw      = data(:,2);
21          idxL    = wl >= leftRange(1) & wl <= leftRange(2);
22          wlL     = wl(idxL);
23          pwL     = filtfilt(b, a, pw(idxL));
24          plot(ax1, wlL, pwL, 'LineWidth', 1.5);
25          end
26          hold(ax1,'off');
27          title(ax1,'Smoothed Left Sidelobe');
28          xlabel(ax1,'Wavelength (nm)');
29          ylabel(ax1,'Power (dB)');
30          grid(ax1,'on');
31          grid(ax1,'minor');
32
33          ax2 = nexttile;
34          hold(ax2,'on');
35          for i = 1:nFiles
36          data    = readmatrix(files{i});
37          wl      = data(:,1);
38          pw      = data(:,2);
39          idxR    = wl >= rightRange(1) & wl <= rightRange(2);
40          wlR     = wl(idxR);
41          pwR     = filtfilt(b, a, pw(idxR));
42          plot(ax2, wlR, pwR, 'LineWidth', 1.5);
43          end
44          hold(ax2,'off');
45          title(ax2,'Smoothed Right Sidelobe');
46          xlabel(ax2,'Wavelength (nm)');
47          ylabel(ax2,'Power (dB)');
48          grid(ax2,'on');
49          grid(ax2,'minor');
```

Listing A.5: Smoothed Sidelobes.